Arabian Journal of Chemistry (2015) **xxx**, xxx–xxx

King Saud University

Arabian Journal of Chemistry

www.ksu.edu.sa
www.sciencedirect.com

ORIGINAL ARTICLE

Synthesis of heterocyclic compounds and its applications

Mohan N. Patel *, Parag S. Karia, Pankajkumar A. Vekariya, Anshul P. Patidar

Department of Chemistry, Sardar Patel University, Vallabh Vidyanagar 388 120, Gujarat, India

Received 28 February 2015; accepted 26 June 2015

KEYWORDS

Heterocyclic compound;
Ruthenium(II) complexes;
Nucleic acid intercalating agent;
Cytotoxicity

Abstract The octahedral ruthenium(II) complexes $[Ru(L^n)(PPh_3)_2Cl_2]$ [L^n = biphenyl furanyl pyridine derivatives] were synthesized and characterized using LC–MS, IR spectroscopy, elemental analysis and magnetic measurements. Complexes show enhancement in antibacterial activity compared to free ligands. From the binding mode investigation by absorption titration and viscosity measurement, it is observed that complexes bind to DNA via intercalation and also complexes promote the cleavage of supercoiled pUC19 plasmid DNA. Cytotoxicity analysis shows 100% mortality of Brine shrimp after 48 h.

1. Introduction

Recently, metal complexes as DNA interacting agents have been talk in medicinal inorganic chemistry (Fei et al., 2014; Zhao et al., 2011; Abou-Hussen and Linert, 2009; Patel, 2004; Wu et al., 2011; Khan et al., 2014). DNA intrastrand cross-linking agents are found useful in treatment of cancers, psoriasis and various anemias. Several ruthenium complexes have been developed as an alternative to *cis*-platin as potential anticancer agents with lower toxicity than the platinum counterparts (Clarke and Keppler, 1993; Keppler et al., 1993; Clarke et al., 1999; Sava and Bergamo, 2000). Large interest has been drawn toward the interaction of Ru(II) complexes containing planar polycyclic hetero aromatic ligands (Ji et al., 2001). Studies on DNA-binding of the complexes are crucial in development of nucleic acid interaction, chemotherapy and photodynamic treatment (Huppert, 2008; Balasubramanian and Neidle, 2009; Georgiades et al., 2010). Recently, ruthenium(II) polypyridyl complexes have been found to induce apoptosis in A549 cells (Bing-Jie et al., 2014). Also, the main ligands of Ru(II)–polypyridyl complexes possess extended conjugated planar aromatic structures can insert and stack between the base pairs of DNA. Considerable effects are observed in the binding mode, sites and affinities upon slight changes in the molecular structures of Ru(II) complexes which provide the opportunity to discover important information on site-specific DNA probes. Therefore, studies on modifying the main ligand is quite significant for understanding the optical properties of DNA-binding and action mechanism of ruthenium complexes.

In continuation of our earlier work (Patel et al., 2014), biological activity of the synthesized complexes was carried out by performing antibacterial, DNA binding, DNA cleavage and cytotoxicity study.

* Corresponding author. Tel.: +91 (2692) 226856x218.
E-mail address: jeenen@gmail.com (M.N. Patel).

Peer review under responsibility of King Saud University.

ELSEVIER Production and hosting by Elsevier

http://dx.doi.org/10.1016/j.arabjc.2015.06.031

2. Experimental

2.1. Reagents and materials

All the chemicals were of analytical grade. Ruthenium chloride trihydrate, 2-acetylfuran, 4-chlorobenzaldehyde, 4-fluorobezaldehyde, 4-bromobezaldehyde, 3-chlorobenzaldehye, 3-fluorobezaldehyde and 3-bromobezaldehyde were purchased from Sigma Chemical Co. (India). Ethidium bromide (EB), bromophenol blue, agarose and Luria Broth (LB) were purchased from Himedia (India). Culture of pUC19 bacteria (MTCC 47) was purchased from Institute of Microbial Technology (Chandigarh, India).

2.2. Physical measurements

Perkin–Elmer 240 Elemental Analyzer was used to collect micro analytical data. Room temperature magnetic susceptibility was measured by Gouy's method. FT–IR data were collected by FT–IR ABB Bomen MB 3000 spectrophotometer. The ^{1}H NMR and ^{13}C NMR were recorded on a Bruker Avance (400 MHz). UV–Vis spectra of the complexes were recorded on UV-160A UV–Vis spectrophotometer, Shimadzu (Japan). Cleavage of pUC19 DNA was quantified by AlphaDigiDoc™ RT. Version V.4.0.0.

2.3. Synthesis of ligands

Modification of Krohnke pyridine synthesis (Krohnke, 1976) has been used for the synthesis of ligands **[L^1–L^6]** (Scheme 1).

2.3.1. Synthesis of 4-(4-fluorophenyl)-2-(furan-2-yl)-6-p-tolylpyridine [L^1]

Substituted enone synthesized by the reaction of *p*-fluorobenzaldehyde and *p*-methylacetophenone, was refluxed with pyridinium salt of 2-acetylfuran in presence of ammonium acetate for 6 h. The reaction mixture was allowed to cool at room temperature. The solid product was filtered and recrystallized from hexane. **Yield:** 53%, **mp:** 118 °C, **Anal. Calc.** for $C_{22}H_{16}FNO$ (329.37): **Calc. (%):** C, 80.23; H, 4.90; N, 4.25. **Found (%):** C, 80.21; H, 4.93; N, 4.27. **^{1}H NMR ($CDCl_3$, 400 MHz):** δ (ppm) 8.068–8.064 (d-poor resolved, 2H, $H_{2'',6''}$), 7.823–7.819 (d, 1H, H_3), 7.765–7.730 (complex, 3H, $H_{5,3'',5''}$), 7.590–7.584 (dd-poor resolved, 1H, $H_{5'}$), 7.345–7.325 (d, 2H, $H_{3''',5'''}$), 7.284–7.209 (complex, 3H, $H_{4',2''',6'}$), 6.606–6.593 (dd, 1H, $H_{3'}$), 2.456 (s, 3H, —CH_3). **IR (KBr, 4000–400 cm^{1}):** 3032, ν(C—H)$_{ar\ stretching}$; 1543, ν(C=C); 1497, ν(C=N); 1304, pyridine skeleton band; 1220, ν(C—F); 918, 818, (*p*-substituted ring); 740, ν(C—H)$_{ar\ bending}$. **^{13}C NMR ($CDCl_3$, 100 MHz) δ (ppm):** 157.19 ($C_{4''}$), 155.83 (C_2), 149.96 ($C_{6,2'}$), 143.04 (C_4), 139.37 ($C_{5'}$), 136.88 ($C_{1''}$), 131.48 ($C_{1'''}$), 129.44 ($C_{2'',6'',4'''}$), 128.14 ($C_{3''',5'''}$), 124.12 ($C_{3,2''',6'''}$), 116.41 ($C_{3'}$), 114.78 ($C_{3'',5''}$), 112.25 (C_5), 109.07 ($C_{4'}$), 20.53 —CH_3.

2.3.2. Synthesis of 4-(4-chlorophenyl)-2-(furan-2-yl)-6-p-tolylpyridine [L^2]

It has been synthesized using pyridinium salt of 2-acetyl furan and the enone prepared by the reaction between *p*-chlorobenzaldehyde and *p*-methylacetophenone. **Yield:** 59%, **mp:** 110 °C, **Anal. Calc.** for $C_{22}H_{16}ClNO$ (345.82): **Calc. (%):** C, 76.41; H, 4.66; N, 4.05. **Found (%):** C, 76.44; H, 4.67; N, 4.08. **^{1}H NMR ($CDCl_3$, 400 MHz):** δ (ppm) 8.064–8.044 (dd,

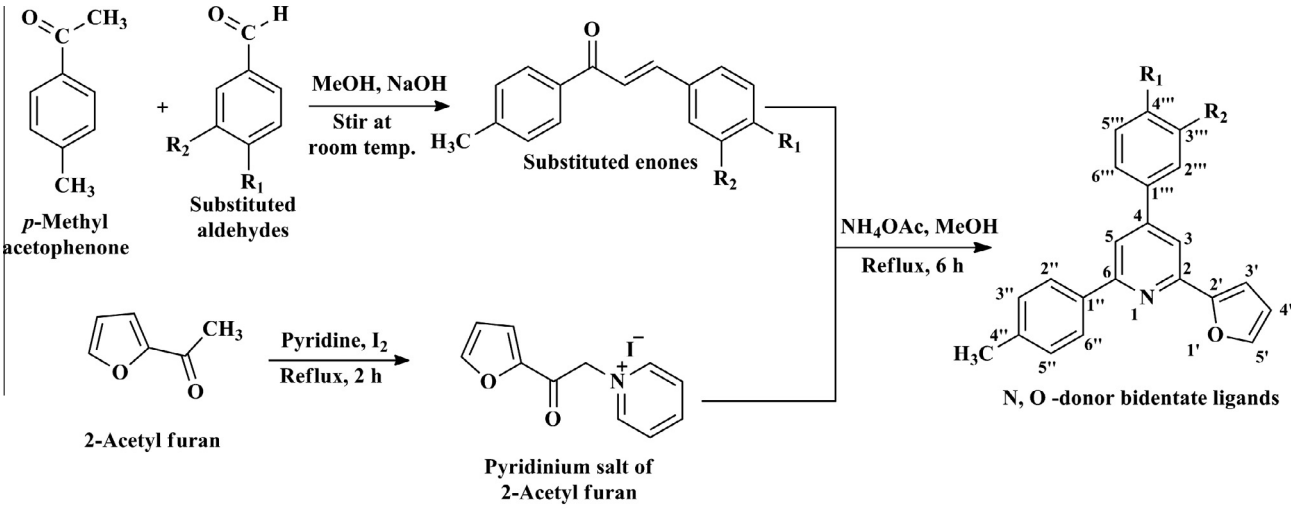

Ligands	R_1	R_2
L^1	F	H
L^2	Cl	H
L^3	Br	H
L^4	H	F
L^5	H	Cl
L^6	H	Br

Scheme 1 General reaction scheme for the synthesis of ligands.

2H, $H_{2'',6''}$), 7.823–7.821 (dd, 1H, $H_{5'}$), 7.757 (s, 1H, H_3), 7.714–7.693 (d, 2H, $H_{3''',5'''}$), 7.588 (s, 1H, H_5), 7.524–7.503 (d, 2H, $H_{3'',5''}$), 7.345–7.325 (d, 2H, $H_{2''',6'''}$), 7.284–7.271 (dd, 1H, $H_{4'}$), 6.606–6.594 (dd, 1H, $H_{3'}$), 2.456 (s, 3H, $-CH_3$). **IR (KBr, 4000–400 cm^{-1}):** 3063, ν(C—H)$_{ar\ stretching}$; 1543, ν(C=C); 1489, ν(C=N); 1327, pyridine skeleton band; 1040, ν(C—Cl); 987, 810, (*p*-substituted ring) 733, ν(C—H)$_{ar\ bending}$. **^{13}C NMR (CDCl$_3$, 100 MHz) δ (ppm):** 156.52 ($C_{4''}$), 154.13 (C_2), 150.83 ($C_{2'}$), 144.66 (C_6), 139.89 (C_4), 138.54 ($C_{5'}$), 136.11 ($C_{1'',1'''}$), 132.60 ($C_{2'',6'',4'''}$), 130.22 ($C_{3,3''',5'''}$), 128.61 ($C_{2''',6'''}$), 126.40 ($C_{3'',5''}$), 124.08 (C_5), 117.52 ($C_{4'}$), 115.91 ($C_{3'}$), 20.66 —CH_3.

2.3.3. Synthesis of 4-(4-bromophenyl)-2-(furan-2-yl)-6-p-tolylpyridine [L^3]

It has been synthesized using the pyridinium salt of 2-acetyl furan and enone prepared by the reaction between *p*-bromobenzaldehyde and *p*-methylacetophenone. **Yield:** 49%, **mp:** 130 °C, **Anal. Calc.** for $C_{22}H_{16}BrNO$ (390.27): **Calc. (%):** C, 67.71; H, 4.13; N, 3.59. **Found (%):** C, 67.74; H, 4.17; N, 3.61. **^{1}H NMR (CDCl$_3$, 400 MHz):** δ (ppm) 8.071–8.051 (d, 2H, $H_{2'',6''}$), 7.968–7.948 (dd, 1, $H_{5'}$), 7.831 (s, 1H, H_3), 7.792 (s, 1H, H_5), 7.580–7.539 (t, $3H_{2''',3''',6'''}$), 7.500 (s poor resolved, 1H, $H_{5'''}$), 7.335–7.240 (complex, 3H, $H_{4',3'',5''}$), 6.607–6.597 (dd, 1H, $H_{3'}$), 2.420 (s, 3H, —CH_3). **IR (KBr, 4000–400 cm^{-1}):** 3044, ν(C—H)$_{ar\ stretching}$; 1543, ν(C=C); 1427, ν(C=N); 1373, pyridine skeleton band; 1050, ν(C—Br); 920, 818, (*p*-substituted ring); 771, ν(C—H)$_{ar\ bending}$. **^{13}C NMR (CDCl$_3$, 100 MHz) δ (ppm):** 157.64 ($C_{4''}$), 155.01 (C_2), 150.05 ($C_{2'}$), 148.01 (C_6), 143.01 (C_4), 140.76 ($C_{5'}$), 139.50 ($C_{1''}$), 136.51 ($C_{1'''}$), 135.17 ($C_{2''}$), 130.14 ($C_{6''}$), 129.88 ($C_{3''',4''',5'''}$), 126.88 ($C_{3,3'',5''}$), 124.90 ($C_{2'''}$), 117.08 ($C_{6'''}$), 115.11 (C_5), 112.52 ($C_{4'}$), 108.37 ($C_{3'}$), 20.54 —CH_3.

2.3.4. Synthesis of 4-(3-fluorophenyl)-2-(furan-2-yl)-6-p-tolylpyridine [L^4]

It has been synthesized using the pyridinium salt of 2-acetyl furan and enone prepared by the reaction between *m*-fluorobenzaldehyde and *p*-methylacetophenone. **Yield:** 59%, **mp:** 90 °C, **Anal. Calc. for:** $C_{22}H_{16}FNO$ (329.37): **Calc. (%):** C, 80.23; H, 4.90; N, 4.25. **Found (%):** C, 80.24; H, 4.88; N, 4.27. **^{1}H NMR (CDCl$_3$, 400 MHz):** δ (ppm) 8.075–8.054 (d, 2H, $H_{2'',6''}$), 7.839–7.836 (d, 1H, H_3), 7.774–7.771 (d, 1H, H_5), 7.597–7.593 (d, 1H, $H_{5'''}$), 7.566–7.454 (complex, 3H, $H_{2''',4''',6'''}$), 7.350–7.330 (d, 2H, $H_{3'',5''}$), 7.283–7.274 (d-poor resolved, 1H, $H_{5'}$), 7.211–7.164 (t-poor resolved, 1H, $H_{4'}$), 6.610–6.592 (dd, 1H, $H_{3'}$), 2.459 (s, 3H, —CH_3). **IR (KBr, 4000–400 cm^{-1}):** 3063, ν(C—H)$_{ar\ stretching}$; 1551, ν(C=C); 1489, ν(C=N); 1381, pyridine skeleton; 1222, ν(C—F). **^{13}C NMR (CDCl$_3$, 100 MHz) δ (ppm):** 157.11 ($C_{3''}$), 154.1 (C_2), 149.96 ($C_{2'}$), 148.51 (C_6), 143.88 ($C_{4'}$), 139.07 ($C_{1''}$), 137.05 ($C_{5'}$), 130.98 ($C_{1'''}$), 129.43 ($C_{3''',5'''}$), 128.86 ($C_{4'''}$), 127.08 ($C_{5'',2''',6'''}$), 123.32 ($C_{6''}$), 116.45 ($C_{3,5}$), 114.06 ($C_{4'}$), 112.67 ($C_{2'',4''}$), 109.07 ($C_{3'}$), 20.67 —CH_3.

2.3.5. Synthesis of 4-(3-chlorophenyl)-2-(furan-2-yl)-6-p-tolylpyridine [L^5]

It has been synthesized using the pyridinium salt of 2-acetyl furan and enone prepared by the reaction between *m*-chlorobenzaldehyde and *p*-methylacetophenone. **Yield:** 70%, **mp:** 78 °C, **Anal. Calc.** for $C_{22}H_{16}ClNO$ (345.82): **Calc. (%):** C, 76.41; H, 4.66; N, 4.05. **Found (%):** C, 76.40; H, 4.68; N, 4.04. **^{1}H NMR (CDCl$_3$, 400 MHz):** δ (ppm) 8.072–8.052 (d, 2H, $H_{2'',6''}$), 7.910–7.901(t, 1H, H_3), 7.820–7.817 (d, 1H, H_5), 7.756–7.753 (d, 1H, $H_{2'''}$), 7.700–7.681 (d, 1H, $H_{6'''}$), 7.630–7.595 (complex, 2H, $H_{3''',5'''}$), 7.433–7.394 (t, 1H, $H_{4'}$), 7.348–7.329 (d, 2H, $H_{3'',5''}$), 7.248–7.275 (d-poor resolved, 1H, $H_{5'}$), 6.609–6.597 (dd, 1H, $H_{3'}$), 2.458 (s, 3H, —CH_3). **IR (KBr, 4000–400 cm^{-1}):** 3063, ν(C—H)$_{ar\ stretching}$; 1551, ν(C=C); 1489, ν(C=N); 1381, pyridine skeleton band; 1225, ν(C—Cl); 864,748, (*m*-substituted ring). **^{13}C NMR (CDCl$_3$, 100 MHz) δ (ppm):** 156.54 ($C_{3''}$), 154.02 (C_2), 150.00 ($C_{2'}$), 143.51 (C_6), 139.05 (C_4), 138.08 ($C_{1''}$), 135.50 ($C_{5'}$), 132.01 ($C_{1''',4'''}$), 130.00 ($C_{3''',5'''}$), 128.47 ($C_{5'',2''',6'''}$), 126.03 ($C_{2'',4'',6''}$), 123.40 ($C_{3,5}$), 116.50 ($C_{4'}$), 115.17 ($C_{3'}$), 21.44 —CH_3.

2.3.6. Synthesis of 4-(3-bromophenyl)-2-(furan-2-yl)-6-p-tolylpyridine [L^6]

It has been synthesized using the pyridinium salt of 2-acetyl furan and enone prepared by the reaction between *m*-bromobenzaldehyde and *p*-methylacetophenone. **Yield:** 38%, **mp:** 88 °C, **Anal. Calc.** for $C_{22}H_{16}BrNO$ (390.27): **Calc. (%):** C, 67.71; H, 4.13; N, 3.59. **Found (%):** C, 67.75; H, 4.14; N, 3.58. **^{1}H NMR (CDCl$_3$, 400 MHz):** δ (ppm) 8.073–8.053 (d, 2H, $H_{2'',6''}$), 7.830–7.827 (d, 1H, H_3), 7.765–7.750 (dd-poor resolved, $2H_{2''',6'''}$), 7.660–7.634 (complex, 1H, $H_{4'}$), 7.596–7.594 (dd-poor resolved, 1H, H_5), 7.480–7.464 (complex, 2H, $H_{3''',5'''}$), 7.349–7.329 (d, 2H, $H_{3'',5''}$), 7.288–7.284 (d-poor resolved, 1H, $H_{5'}$), 6.610–6.597 (dd, 1H, $H_{3'}$), 2.458 (s, 3H, —CH_3). **IR (KBr, 4000–400 cm^{-1}):** 3063, ν(C—H)$_{ar\ stretching}$; 1543, ν(C=C); 1497, ν(C=N); 1381, pyridine skeleton band; 1369, ν(C—Br); 813,733, (*m*-substituted ring). **^{13}C NMR (CDCl$_3$, 100 MHz) δ (ppm):** 158.01 ($C_{3''}$), 154.52 (C_2), 149.97 ($C_{2'}$), 148.81 (C_6), 143.10 (C_4), 139.11 ($C_{1''}$), 136.66 ($C_{5'}$), 130.09 ($C_{1'''}$), 129.54 ($C_{3''',5'''}$), 128.44 ($C_{4'''}$), 127.58 ($C_{5'',2''',6'''}$), 122.67 ($C_{6''}$) 116.40 ($C_{3,5}$). 114.88 ($C_{2'',4''}$), 112.32 ($C_{4'}$), 109.06 ($C_{3'}$), 20.91 —CH_3.

2.4. Synthesis of complexes

A ruthenium precursor [$RuCl_3(PPh_3)_3$] was prepared by refluxing the methanolic solution of $RuCl_3 \bullet 3H_2O$ and PPh_3 (1:3) in presence of conc. HCl for 1 h. The obtained reddish brown precipitate was filtered and dried under vacuum.

2.4.1. Synthesis of [$Ru(L^1)(PPh_3)_2Cl_2$] (1)

It has been synthesized by refluxing the solution of ruthenium precursor [$RuCl_3(PPh_3)_3$] in toluene (0.1 mmol) with the methanolic solution of ligand 4-(4-fluorophenyl)-2-(furan-2-yl)-6-*p*-tolylpyridine [L^1] (0.1 mmol) in presence of LiCl as a reducing agent (0.4 mmol in methanol) and Et_3N (0.1 mmol in methanol) for 4 h. The resulting solution has been concentrated to half of its volume and the product has been separated by adding small amount of pet ether (60:80). The obtained blackish brown product was washed with methanol, toluene and dried under vacuum (Scheme 2). **Yield:** 12.5%, **mp:** 272.2 °C, **Anal. Calc.** for: $C_{58}H_{46}Cl_2FNOP_2Ru$ (1025.91): **Calc. (%):** C, 67.90; H, 4.52; N, 1.37; Ru, 9.85. **Found (%):** C, 67.84; H, 4.53; N, 1.45; Ru$_{(gravimetrically)}$, 9.80. **UV–Vis (In DMSO):** λ (nm) (ε, M^{-1} cm^{-1}): (In DMSO): 550 (450), 385 (4365), 275 (23,850). **Conductance:** 11 Ω^{-1} cm^2 mol^{-1}.

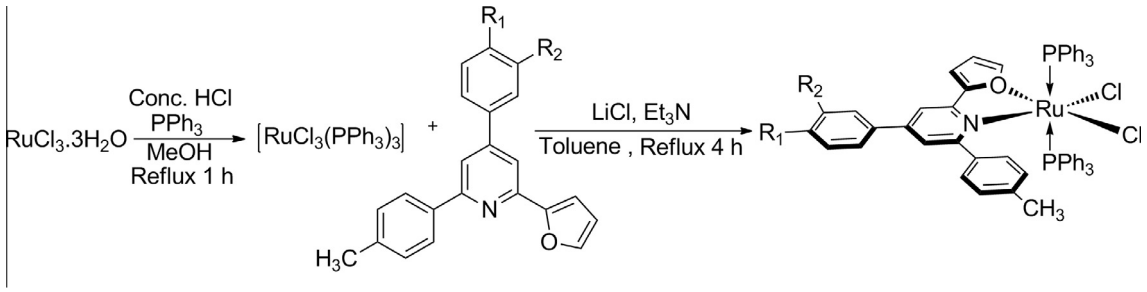

Complex	R_1	R_2
I	F	H
II	Cl	H
III	Br	H
IV	H	F
V	H	Cl
VI	H	Br

Scheme 2 Reaction scheme for the synthesis of complexes.

2.4.2. Synthesis of $[Ru(L^2)(PPh_3)_2Cl_2]$ (II)

It has been synthesized using ligand 4-(4-chlorophenyl)-2-(furan-2-yl)-6-*p*-tolylpyridine. **Yield:** 11.92%, **mp:** 256.1 °C, **Anal. Calc.** for: $C_{58}H_{46}Cl_3NOP_2Ru$ (1042.37): **Calc. (%):** C, 66.83; H, 4.45; N, 1.34; Ru, 9.70. **Found (%):** C, 67.00; H, 4.43; N, 1.31; $Ru_{(gravimetrically)}$, 9.78. UV–Vis λ_{max} (nm) (In DMSO): **UV–Vis (In DMSO):** λ (nm) (ε, M^{-1} cm^{-1}): (In DMSO): 562 (380), 410 (5732), 272 (17,650). **Conductance:** 24 Ω^{-1} cm^2 mol^{-1}.

2.4.3. Synthesis of $[Ru(L^3)(PPh_3)_2Cl_2]$ (III)

It has been synthesized using the ligand 4-(4-bromophenyl)-2-(furan-2-yl)-6-*p*-tolylpyridine. **Yield:** 9.9%, **mp:** 284.5 °C, **Anal. Calc.** for: $C_{58}H_{46}BrCl_2NOP_2Ru$ (1086.82): **Calc. (%):** C, 64.10; H, 4.27; N, 1.29; Ru, 9.30. **Found (%):** C, 67.24; H, 4.23; N, 1.23; $Ru_{(gravimetrically)}$, 9.35. **UV–Vis (In DMSO):** λ (nm) (ε, M^{-1} cm^{-1}): 582 (260), 398 (7340), 273 (11,440). **Conductance:** 7 Ω^{-1} cm^2 mol^{-1}.

2.4.4. Synthesis of $[Ru(L^4)(PPh_3)_2Cl_2]$ (IV)

It has been synthesized using the ligand 4-(3-fluorophenyl)-2-(furan-2-yl)-6-*p*-tolylpyridine. **Yield:** 13.4%, **mp:** 287.8 °C, **Anal. Calc.** for: $C_{58}H_{46}Cl_2FNOP_2Ru$ (1025.91): **Calc. (%):** C, 67.90; H, 4.52; N, 1.37; Ru, 9.85. **Found (%):** C, 67.82; H, 4.50; N, 1.43; $Ru_{(gravimetrically)}$, 9.87. **UV–Vis (In DMSO):** λ (nm) (ε, M^{-1} cm^{-1}): 574 (387), 408 (5540), 270 (20,980). **Conductance:** 14 Ω^{-1} cm^2 mol^{-1}.

2.4.5. Synthesis of $[Ru(L^5)(PPh_3)_2Cl_2]$ (V)

It has been synthesized using the ligand 4-(3-chlorophenyl)-2-(furan-2-yl)-6-*p*-tolylpyridine. **Yield:** 13.5%, **mp:** 268.4 °C, **Anal. Calc.** for: $C_{58}H_{46}Cl_3NOP_2Ru$ (1042.37): **Calc. (%):** C, 66.83; H, 4.45; N, 1.34; Ru, 9.70. **Found (%):** C, 66.90; H, 4.40; N, 1.30; $Ru_{(gravimetrically)}$, 9.63. **UV–Vis (In DMSO):** λ (nm) (ε, M^{-1} cm^{-1}): 563 (387), 389 (6252), 272 (16,440). **Conductance:** 32 Ω^{-1} cm^2 mol^{-1}.

2.4.6. Synthesis of $[Ru(L^6)(PPh_3)_2Cl_2]$ (VI)

It has been synthesized using the ligand 4-(3-bromophenyl)-2-(furan-2-yl)-6-*p*-tolylpyridine. **Yield:** 9.0%, **mp:** 264.1 °C, **Anal. Calc.** for: $C_{58}H_{46}BrCl_2NOP_2Ru$ (1086.82): **Calc. (%):** C, 64.10; H, 4.27; N, 1.29; Ru, 9.30. **Found (%):** C, 67.15; H, 4.29; N, 1.25; $Ru_{(gravimetrically)}$, 9.26. **UV–Vis (In DMSO):** λ (nm) (ε, M^{-1} cm^{-1}): 558 (270), 392 (8120), 275 (15,427). **Conductance:** 19 Ω^{-1} cm^2 mol^{-1}.

2.5. Broth dilution method – an in vitro antibacterial study

The MIC informs about the degree of resistance of certain bacterial species toward the test compounds. MIC was performed by serially twofold dilution of the test compound added to two $Gram^{(+ve)}$ (*Bacillus subtilis* and *Serratia marcescens*) and three $Gram^{(-ve)}$ (*Escherichia coli*, *Pseudomonas aeruginosa* and *Staphylococcus aureus*) and incubated at optimum temperature for 24 h. If after 24 h bacterial growth is observed double of the previously added concentration was taken for the test compounds in tube and incubated for 24 h again. A concentration at which no visible growth of bacteria is observed in the tubes is regarded as minimum inhibitory concentration (MIC) at which bacteria cannot defend against the test compounds.

2.6. DNA binding mode study

Binding mode of complex on interacting to DNA can be investigated by the alteration occurred in the absorption spectral titration. This titrimetric analysis was performed by varying the concentration of the HS–DNA with the addition of 100 μL of its aliquots in each successive addition in reference cell and sample cell, keeping the complex concentration constant, with the due correction for the absorbance of HS–DNA alone. Spectra were recorded after 10 min of incubation (Usharani et al., 2013).

Further the confirmation of binding mode was done from the viscosity measurement technique. An increase in viscosity of native DNA upon binding of complexes is regarded as diagnostic feature of an intercalation process. The binding mode of

present compounds was investigated by taking the HS–DNA solution of 200 μM in Ubbelohde viscometer maintained in constant thermometric bath. The time for DNA alone (t_o) and for successive addition of the complex (t) were monitored.

2.7. BSLA – In vitro cytotoxicity assay

All the complexes were screened for in vitro toxicity using the protocol of Mayer et al., as an initial step for the discovering new drug. This method allows the use of fewer amounts of test compounds and permits a large number of samples and dilutions within a shorter time for analysis. From these stock solutions of 1000 μg/mL; a set of 2, 4, 8, 12, 16 and 20 μg/mL was prepared. Three such replicates for each test compounds along with the control containing DMSO alone were prepared. After 24 h the number of survivals was counted (Meyer et al., 1982). A graph of log of concentration of samples was plotted against percentage of mortality of nauplii (Islam et al., 2007). The LC_{50} value is the antilogarithm of [complex] corresponding to the 50% mortality.

2.8. DNA nuclease profile

Gel electrophoresis technique is widely used to study the cleavage of DNA by the action of test compounds. Isolated pUC19 DNA was subjected to agarose gel electrophoresis to investigate the cleavage ability of ruthenium(II) complexes. An aliquot of 10 μL pUC19 DNA and 5 μL ruthenium(II) complexes **(1–6)** were kept for incubation at 37 °C for 4 h and electrophoresed after addition of bromophenol blue for 2 h at 100 V on 1% agarose gel using Tris–acetic acid–EDTA (TAE) buffer (pH 7.2). Ethidium bromide was added to TAE buffer as a staining agent. After electrophoresis the gel was photographed under UV illuminator. Quantification of DNA cleavage in terms of% cleavage is achieved from the gel electrophoresis experiment.

3. Results and discussion

3.1. Electronic spectra and magnetism

The electronic spectra of all the complexes were obtained using DMSO as a solvent. Three distinct bands are observed in the range of 240–800 nm. The band in the range of 270–275 nm is the characteristic intra ligand charge transfer band as the extinction coefficient is found to be higher than 10,000 unit, which corresponds to the π–π^* transition of ligands. The band around 385–410 nm is due to metal to ligand charge transfer band as the extinction coefficient fall in the range of 1000–10,000. The peak around 550–582 nm is due to d–d transition as the extinction coefficient is in the range of 100–1000 unit (Balasubramanian et al., 2007). The d–d transition is weakly intense on the spectrum as they are Laporte forbidden. The ground state of Ru(II) in an octahedral field (t_{2g}^6 configuration) is $^1A_{lg.}$ The excited states corresponding to $t_{2g}^5 e_g^1$ configuration are $^3T_{lg}$, $^3T_{2g}$, $^1T_{1g}$ and $^1T_{2g}$ in increasing order of energy. Thus, one should expect four transitions (Gunasekaran et al., 2012). But all the transitions are not observed in the actual spectrum as their intensities are very low. The electronic spectrum of complex-**(I)** is represented in the supplementary material. The magnetic moment of all the complexes is found to be zero indicating the absence of unpaired electron in a low-spin d^6 – configuration (t_{2g}^6) for Ru(II) ion in octahedral environment.

3.2. Infrared spectroscopic characterization of complexes

IR spectral data of free ligands (Section 2.3) are compared with their respective ruthenium(II) complexes (Table 1) to confirm whether the ligand has coordinated to ruthenium(II) ion or not. The peaks corresponding to the ring stretching frequencies of ν(C═N) of ligands (1427–1497 cm^{-1}) were shifted to higher frequencies upon complexation (1504–1518 cm^{-1}) indicating the coordination of the heterocyclic nitrogen atoms to metal ion (Reddy and Shilpa, 2011). Bands observed in the of range 1546–1556 cm^{-1} are assigned as $\nu(C{=}C)_{ar.}$ The $(C{-}H)_{ar.}$ stretching bands are observed in the range of 3029–3057 cm^{-1}. Bands observed in the range of 547–567 cm^{-1} and 446–464 cm^{-1} are assigned due to ν(Ru—N) and ν(Ru—O) stretching vibration, respectively.

3.3. Thermogravimetric decomposition analysis of complexes

Fig. 1 shows the TG curve for complex-**(I)** obtained at a heating rate of 10 °C per minute in the temperature range of 0–900 °C under N_2 atmosphere. No decomposition up to 130 °C suggests the absence of water molecule in the complex. First mass loss (6.93%) in the temperature range of 130–240 °C corresponds to loss of chlorine atoms. Second mass loss (51.11%) in the range of 30–590 °C corresponds to the loss of triphenylphosphine moiety. The third mass loss (32.09%) in the range of 660–780 °C corresponds to the loss of neutral bidentate ligand, thus leaving behind metal oxide as a residue.

3.4. Mass spectra

The mass spectrum of complex-**(I)** (Fig. 2) shows that molecular ion peaks at m/z = 1025.09, 1027.01 and 1029.05 are assigned to (M^+), (M + 2), and (M + 4), due to the presence

Table 1 IR spectra of complexes.

Sr. no.	$\nu(C{=}N)_{ar}$ (cm^{-1})	$\nu(C{=}C)_{ar}$ (cm^{-1})	$\nu(C{-}H)_{ar}$ (cm^{-1})	ν(Ru—N) (cm^{-1})	ν(Ru—O) (cm^{-1})	PPh_3 (cm^{-1})
(I)	1512	1549	3029	554	446	1450, 1039, 691
(II)	1506	1546	3040	549	459	1451, 1034, 694
(III)	1518	1548	3038	548	464	1451, 1037, 689
(IV)	1518	1554	3038	567	450	1448, 1029, 695
(V)	1504	1552	3044	550	458	1429, 1024, 686
(VI)	1514	1556	3057	547	460	1428, 1022, 684

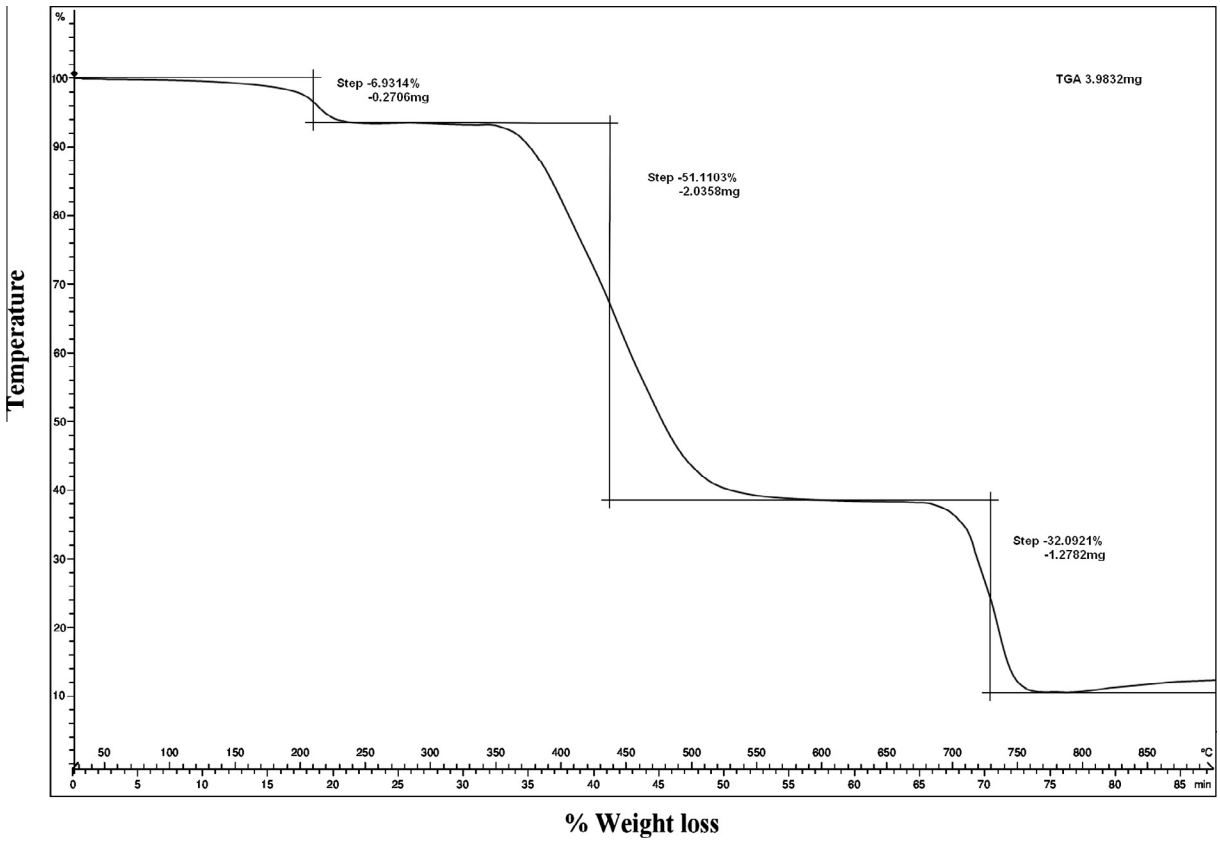

Figure 1 Thermogram of complex-**I**.

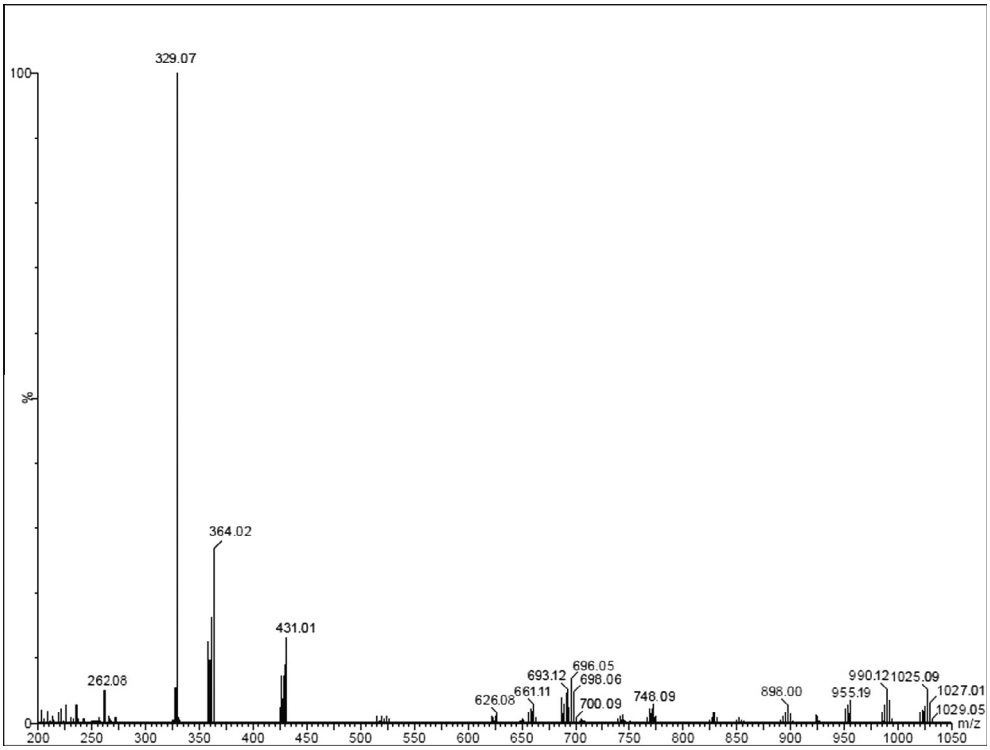

Figure 2 LC–MS spectrum of complex-**I**.

of two chlorine atoms. The peak observed at m/z = 990.12 is due to loss of one chlorine atom. The peak at 955.19 is due to the loss of second chlorine atom. Several other fragments at 898.00, 748.09, 696.05, 693.12, 661.11, 626.08, 431.01, 364.02, 329.07 and 262.07 m/z value are observed, which attributed to fragments associated with complex.

3.5. Broth dilution method – an in vitro antibacterial study

From the result represented in the supplementary material, it is concluded that complex-**(I)** is more potent than the rest of the synthesized complexes. The MIC value of the synthesized complexes is found to be higher than the reference ligands and metal salt, which symbolizes a very superior biological control of bacteria by the synthesized complexes.

3.6. DNA binding mode study

Binding strength of the complexes with DNA is ascertained by UV–Vis absorption titrations, examining the changes in the absorbance of the ligand-centered bands and metal-to-ligand charge transfer bands. Quantification of DNA binding strength is made from K_b values obtained from the ratio of slope to intercept in the graph of [DNA]/(ε_a–ε_f) versus [DNA] represented in the supplementary material. The percentage hypochromism of the complexes is obtained using the equation (A_f–A_b)/A_f, where A_f is the absorbance of fully free form of DNA while A_b is the absorbance of completely bound form in DNA in an experiment. In Fig. 3 hypochromism with red shift is observed suggesting the intercalating mode of binding and the K_b values along with % hypochromism for the complexes are represented in Table 2. The K_b values for the complexes are found in the order of 10^4–10^5 and change in hypochromism of the complexes is found in the range of 16–27%. The values of observed hypochromism and redshift of around 3–4 nm suggests the intercalative mode of binding of complexes (Liu et al., 2008). Obtained K_b value is found higher than $[Ru(dmp)_2(ipbp)]^{+2}$ (dmp = 2,9-dimethyl-1,10-phenanthroline, ipbp = 3-(1H-imidazo[4,5-f][1,10]phenanthrolin-2-yl)-4H-1-banzopyran-2-one) (7.58×10^3 M^{-1})

Table 2 Binding constant (K_b) value of the synthesized complexes.

Sr. no	Complexes	$K_b \times 10^5$ (M^{-1})	% Hypochromism
1	$[Ru(PPh_3)_2(L^1)Cl_2]$ **(I)**	2.60	27.35
2	$[Ru(PPh_3)_2(L^2)Cl_2]$ **(II)**	1.72	25.50
3	$[Ru(PPh_3)_2(L^3)Cl_2]$ **(III)**	1.18	20.47
4	$[Ru(PPh_3)_2(L^4)Cl_2]$ **(IV)**	0.889	18.79
5	$[Ru(PPh_3)_2(L^5)Cl_2]$ **(V)**	0.318	16.66
6	$[Ru(PPh_3)_2(L^6)Cl_2]$ **(VI)**	0.474	16.66

Liu et al., 1999, but lower than the classical intercalators $[Ru(bpy)_2(pip)]^{2+}$ (pip = 2-phenylimidazo[4,5-f][1,10]phenanthroline) (4.70×10^5 M^{-1}) Xie et al., 2013 and $[Ru(dmb)_2(addppn)](ClO_4)_2$ (dmb = 4,4′-dimethyl-2,2′-bipyridine, addppn = acenaphtheno[1,2-b]-1,4-diazabenzo[i]dipyrido[3,2-a:2′,3′-c]phenazine) (4.78×10^5 M^{-1}) Liu et al., 2008.

Viscosity measurement technique solely cannot determine the binding mode of the complex and is used along with the absorption titration measurement to deduce the binding mode. From the average flow time η/η_0 is calculated and plotted against [DNA]/[complex]. In Fig. 4 viscosity of DNA solution increases upon the addition of complexes in varying concentration. From the result of absorption and viscometric studies, it is concluded that complexes bind to DNA via intercalative binding mode.

3.7. BSLA – in vitro cytotoxicity assay

In the brine shrimp lethality bioassay (BSLA), complexes show positive results indicating that the complexes are biologically active. The mortality rate of nauplii is found to increase with increasing concentration of sample. The graph of% mortality versus log conc. and the graph of LC_{50} values of synthesized complexes are represented in Figs. 5 and 6 respectively. From the graph, it can be observed that LC_{50} values of complexes are found in the range of 6.76–19.50 μg/mL.

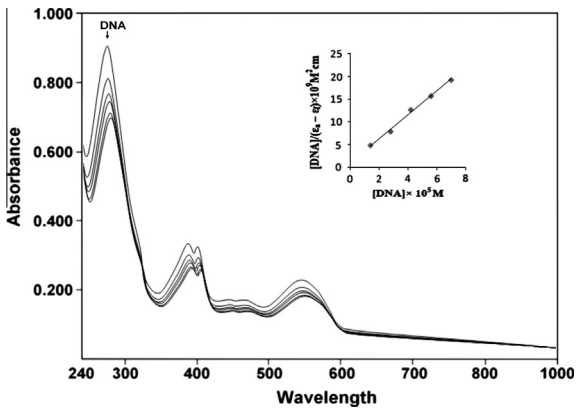

Figure 3 Absorption spectra of complex-**I** with increasing concentration of HS–DNA in phosphate buffer Inset: Plots of [DNA]/(ε_a–ε_f) versus [DNA] for the titration of DNA with ruthenium(III) complexes.

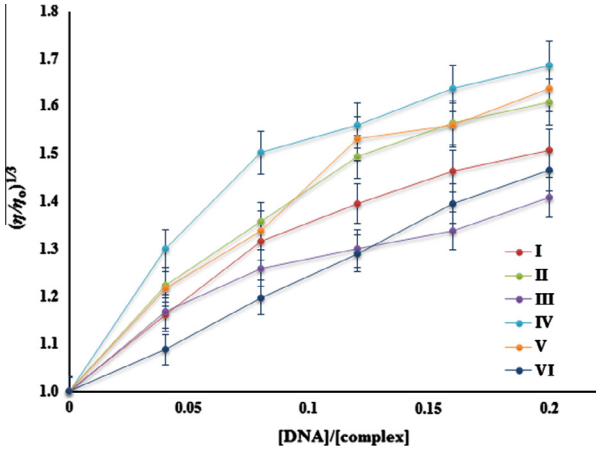

Figure 4 Effect on relative viscosity of DNA under the influence of increasing amount of complexes at 27 ± 0.1 °C in phosphate buffer (Na_2HPO_4/NaH_2PO_4, pH 7.2).

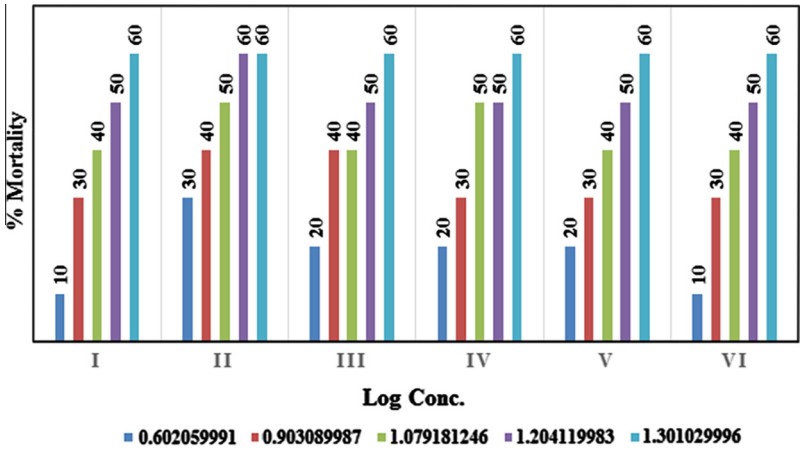

Figure 5 % mortality against the log conc. of the complexes.

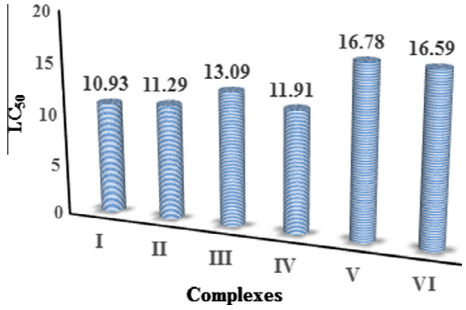

Figure 6 LC_{50} values of the synthesized complexes.

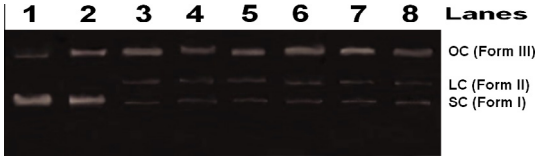

Figure 7 Cleavage of pUC19 plasmid DNA under the influence of ruthenium complexes. Lane 1, DNA control; Lane 2, $RuCl_3 \cdot 3H_2O$; Lane 3, $[Ru(L^1)(PPh_3)_2Cl_2]$; Lane 4, $[Ru(L^2)(PPh_3)_2Cl_2]$; Lane 5, $[Ru(L^3)(PPh_3)_2Cl_2]$; Lane 6, $[Ru(L^4)(PPh_3)_2Cl_2]$; Lane 7, $[Ru(L^5)(PPh_3)_2Cl_2]$; and Lane 8, $[Ru(L^6)(PPh_3)_2Cl_2]$.

3.8. DNA nuclease profile

The DNA cleavage can occur by two major pathways, i.e., hydrolytic and oxidative (Rabindra and Shilpa, 2010). (a) In hydrolytic DNA cleavage, phosphodiester bond undergoes cleavage to generate fragments which can be subsequently referred. Hydrolytic cleavage which started in a modest way of converting supercoil (SC) form of DNA to the open-circular (OC) form and last in linear (L) form, is now being used for identifying the % of cleavage as a function of concentration of nuclease. (b) Oxidative DNA cleavage involves either oxidation of the deoxyribose moiety by abstraction of sugar hydrogen or oxidation of nucleobases. The general mechanism of cleavage of DNA is represented in the supplementary material. Fig. 7 represents the cleavage of DNA taking place from supercoiled (Form I) to open circular (Form III) followed by its scission to linear (Form II). A control experiment using DNA alone does not show any significant cleavage of DNA (Lane 1). A slight cleavage is observed when $RuCl_3 \bullet 3H_2O$ was added to DNA (Lane 2). A significant cleavage of supercoiled form to open circular form is observed (Lane 3–8). The % cleavage data for all the complexes are represented in Table 3. The result clearly suggests that all the complexes cause the efficient scission of pUC19 DNA as compared to the metal salt ($RuCl_3 \bullet 3H_2O$).

Table 3 Gel electrophoresis cleavage data of complexes.

Sr. no	Complexes	% OC	% LC	% SC	% Cleavage
1	Control	13.1	–	86.9	–
2	$RuCl_3 \bullet 3H_2O$	32.3	–	67.8	21.97
3	$[Ru(PPh_3)_2(L^1)Cl_2]$ **(I)**	75.2	14.7	10.2	88.26
4	$[Ru(PPh_3)_2(L^2)Cl_2]$ **(II)**	68.5	10.7	20.2	76.75
5	$[Ru(PPh_3)_2(L^3)Cl_2]$ **(III)**	68.4	15.8	15.7	81.93
6	$[Ru(PPh_3)_2(L^4)Cl_2]$ **(IV)**	79.1	9.6	11.3	86.99
7	$[Ru(PPh_3)_2(L^5)Cl_2]$ **(V)**	71.9	10.4	17.7	79.63
8	$[Ru(PPh_3)_2(L^6)Cl_2]$ **(VI)**	61.2	15.7	23.0	61.09

4. Conclusion

The result of various physicochemical techniques matches well with the theoretically proposed structure of complexes. C, H and N elemental analysis of the complexes matches well with the theoretically proposed structure. Also the result of TGA shows that the decomposition of complex taking place in various steps, supports the percentage data of ligands and PPh_3, indicating the coordination of these ligands to the central metal atom. The different fragment peaks observed in LC–MS spectra support the proof for the theoretically proposed structure of the complexes. MIC of Ru(II) complexes is compared with their respective ligands and it has been observed

that the MIC values of complexes are found to be higher than the corresponding ligands, which may be due to the chelate effect causing increase in the lipophilicity of complexes compared to ligands and hence complexes can easily penetrate the lipid layer of bacterial cell wall and inhibit the bacterial growth. Complex-I binds more efficiently to the DNA than others and result of viscosity measurement reveals that complexes bind to DNA via classical intercalation mode. From the cytotoxicity study, it is found that LC_{50} values of the complexes (10.93–16.78 μg/mL) are lower as compared to reference standard potassium dichromate (32 μg/mL) suggesting that complexes are significantly toxic at low concentration as compared to reference compound and their lower dose can inhibit the 50% of population of test species as compared to the higher dose required for the potassium dichromate. The DNA cleavage study of pUC19 shows that all the complexes show higher % cleavage data (61.09–88.26%) of supercoiled form of pUC19 DNA compared to the reference compound metal salt (21.97%) suggesting an efficient cleavage of pUC19 DNA by the synthesized complexes as compared to the reference compounds metal salt.

Acknowledgements

We are thankful to the Head of chemistry department and UGC RFSMS Scheme for providing financial support.

Appendix A. Supplementary material

Supplementary data associated with this article can be found, in the online version, at http://dx.doi.org/10.1016/j.arabjc.2015.06.031.

References

Abou-Hussen, A., Linert, W., 2009. Chromotropism behavior and biological activity of some schiff base-mixed ligand transition metal complexes. Synth. React. Inorg. Met.-Org. Nano-Met. Chem. 39, 570–599.

Balasubramanian, S., Neidle, S., 2009. G-quadruplex nucleic acids as therapeutic targets. Curr. Opin. Chem. Biol. 13, 345–353.

Balasubramanian, K.P., Karvembu, R., Prabhakaran, R., Chinnusamy, V., Natarajan, K., 2007. Synthesis, spectral, catalytic and antimicrobial studies of PPh_3/$AsPh_3$ complexes of Ru(II) with dibasic tridentate O, N, S donor ligands. Spectrochim. Acta A. 68, 50–54.

Bing-Jie, H., Guang-Bin, J., Wang, J., Wei, L., Hong-Liang, H., Yun-Jun, L., 2014. The studies on bioactivity in *vitro* of ruthenium(II) polypyridyl complexes towards human lung carcinoma A549 cells. RSC Adv. 4, 40899–40906.

Clarke, M.J., Keppler, B.K. (Eds.), 1993. Metal Complexes in Cancer Chemotherapy. VCH, Weinheim, p. 129.

Clarke, M.J., Zhu, F., Frasca, D.R., 1999. Non-platinum chemotherapeutic metallopharmaceuticals. Chem. Rev. 99, 2511–2534.

Fei, B., Xu, W., Tao, H., Li, W., Zhang, Y., Long, J., Liu, Q., Xia, B., Sun, W., 2014. Effects of copper ions on DNA binding and cytotoxic activity of a chiral salicylidene Schiff base. J. Photochem. Photobiol. 132, 36–44.

Georgiades, S.N., Abd Karim, N.H., Suntharalingam, K., Vilar, R., 2010. Interaction of metal complexes with G-Quadruplex DNA. Angew. Chem. Int. Edn. 49, 4020–4034.

Gunasekaran, R., Butcher, R.J., Jayabalakrishnan, C., 2012. Studies on synthesis, characterization, DNA interaction and cytotoxicity of ruthenium(II) Schiff base complexes. Spectrochim. Acta A. 94, 210–215.

Huppert, J.L., 2008. Four-stranded nucleic acids: structure, function and targeting of G-quadruplexes. Chem. Soc. Rev. 37, 1375–1384.

Islam, M.R., Islam, S.M.R., Noman, A.S.M., Khanam, J.A., Ali, S.M.M., Lee, M.W., 2007. Biological screening of a novel nickel (II) tyrosine complex. Mycobiology 35, 25–29.

Ji, L.N., Zou, X.H., Liu, J.G., 2001. Shape- and enantioselective interaction of Ru(II)/Co(III) polypyridyl complexes with DNA. Coord. Chem. Rev. 216, 513–536.

Keppler, B.K., Lipponer, K.G., Stenzel, B., Kratz, F., 1993. In: Keppler, B.K. (Ed.), Metal Complexes Chemotherapy. VCH, Weinheim, pp. 187.

Khan, R., Arjmand, F., Tabassum, S., Monari, M., Marchetti, F., Pettinari, C., 2014. Organometallic ruthenium(II) scorpionate as topo IIα inhibitor; in vitro binding studies with DNA, HPLC analysis and its anticancer activity. J. Organomet. Chem. 771, 47–58.

Krohnke, F., 1976. The specific synthesis of pyridines and oligopyridines. Synthesis 1976, 1–24.

Liu, J.G., Ye, B.H., Li, H., Zhen, Q.X., Ji, L.N., Fu, Y.H., 1999. Polypyridyl ruthenium(II) complexes containing intramolecular hydrogen-bond ligand: syntheses, characterization, and DNA-binding properties. J. Inorg. Biochem. 76, 265–271.

Liu, Y.J., Guan, X.Y., Wei, X.Y., He, L.X., Mei, W.J., Yao, J.H., 2008. Ruthenium(II) complexes containing 2,9-dimethyl-1,10-phenanthroline and 4,4′-dimethyl-2,2′-bipyridine as ancillary ligands: synthesis, characterization and DNA-binding. Tran. Met. Chem. 33, 289–294.

Meyer, B.N., Ferrigni, N.R., Putnam, J.E., Jacobsen, L.B., Nichols, D.E., McLaughlin, J.L., 1982. Brine shrimp: a convenient general bioassay for active plant constituents. Planta Med. 45, 31–34.

Patel, R.N., 2004. Synthesis, spectroscopy, and SOD activity of some imidazolate-bridged copper(II) complexes. Synth. React. Inorg. Met.-Org. Chem. 34, 1041–1055.

Patel, M.N., Patel, C.R., Joshi, H.N., Vekariya, P.A., 2014. Square planar platinum(II) complexes with N, S-donor ligands: synthesis, characterisation, DNA interaction and cytotoxic activity. App. Biochem. Biotechnol. 172, 1846–1858.

Rabindra, R., Shilpa, A., 2010. Interaction of DNA with small molecules: role of copper histidyl peptide complexes in DNA binding and hydrolytic cleavage. Indian J. Chem. 49A, 1003–1015.

Reddy, P., Shilpa, A., 2011. Oxidative and hydrolytic DNA cleavage by Cu(II) complexes of salicylidene tyrosine Schiff base and 1,10 phenanthroline/bipyridine. Polyhedron 30, 565–572.

Sava, G., Bergamo, A., 2000. Ruthenium-based compounds and tumour growth control. Int. J. Oncol. 17, 353–365.

Usharani, M., Akila, E., Rajavel, R., 2013. Evaluation of the pharmacological properties of Schiff base mixed ligand Cu (II), Co (II), Ni (II) and Zn (II) complexes derived from 2-((e)-(4-nitrophenylimino)methyl)phenol. Int. J. Recent Sci. Res. 4, 1385–1390.

Wu, H., Kou, F., Jia, F., Liu, B., Yuan, J., Bai, Y., 2011. A V-shaped ligand 1,3-bis(1-methylbenzimidazol-2-yl)-2-oxapropane and its Cu(II) complex: synthesis, crystal structure, antioxidation and DNA-binding properties. J. Photochem. Photobiol. B 105, 190–197.

Xie, Y.Y., Huang, H.L., Yao, J.H., Lin, G.J., Jiang, G.B., Liu, Y.J., 2013. DNA-binding, photocleavage, cytotoxicity in vitro, apoptosis and cell cycle arrest studies of symmetric ruthenium(II) complexes. Eur. J. Med. Chem. 63, 603–610.

Zhao, P., Huang, J., Ji, L., 2011. Metal complexes of porphyrin–anthraquinone hybrids: DNA binding and photocleavage specificities. J. Coord. Chem. 64, 1977–1990.